Title

The P2Y6 Receptor as a Potential Keystone in Essential Hypertension

Permalink

https://escholarship.org/uc/item/62n99162

Journal

Function, 5(6)

ISSN

2633-8823

Authors

Daghbouche-Rubio, Nuria

Álvarez-Miguel, Inés

Flores, Victor Alejandro

et al.

Publication Date

2024-11-20

DOI

10.1093/function/zqae045

Peer reviewed

ORIGINAL RESEARCH

The P2Y6 Receptor as a Potential Keystone in Essential Hypertension

Nuria Daghbouche-Rubio [1], Inés Álvarez-Miguel [1],
Victor Alejandro Flores[2], Jorge Rojo-Mencía [1], Manuel Navedo [2],
Madeleine Nieves-Citrón [2], Pilar Cidad [1], M. Teresa Pérez-García [1,§],
José R. López-López [1,*,§]

[1]Departamento de Bioquímica y Biología Molecular y Fisiología e Instituto de Biología y Genética Molecular (IBGM), Universidad de Valladolid y Consejo Superior de Investigaciones Científicas (CSIC), Valladolid, 47003, Spain and [2]Department of Pharmacology, University of California Davis, Davis, CA 95616, USA

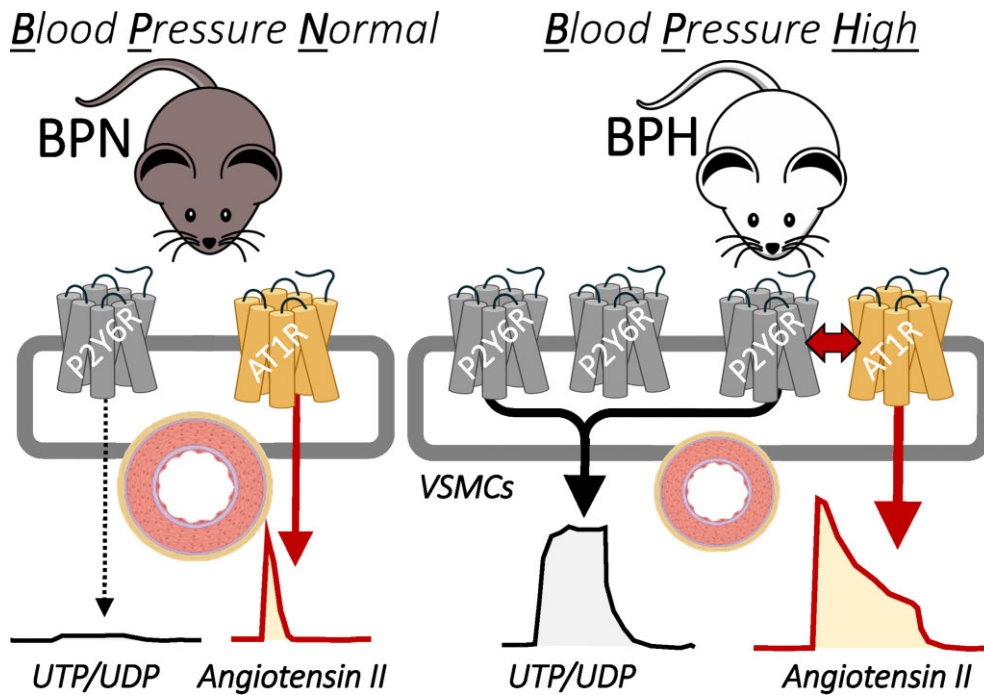*Address correspondence to J.R.L.-L. (e-mail: jrlopez@uva.es)
§Equal senior authors.

Abstract

Essential hypertension (HT) is a highly prevalent cardiovascular disease of unclear physiopathology. Pharmacological studies suggest that purinergic P2Y6 receptors (P2ry6) play important roles in cardiovascular function and may contribute to angiotensin II (AgtII) pathophysiological effects. Here, we tested the hypothesis that functional coupling between P2ry6 and AgtII receptors mediates altered vascular reactivity in HT. For this, a multipronged approach was implemented using mesenteric vascular smooth muscle cells (VSMCs) and arteries from Blood Pressure Normal (BPN) and Blood Pressure High (BPH) mice. Differential transcriptome profiling of mesenteric artery VSMCs identified P2ry6 purinergic receptor mRNA as one of the top upregulated transcripts in BPH. P2Y receptor activation elicited distinct vascular responses in mesenteric arteries from BPN and BPH mice. Accordingly, 10 μM UTP produced a contraction close to half-maximal activation in BPH arteries but no response in BPN vessels. AgtII-induced contraction was also higher in BPH mice despite having lower AgtII receptor type-1 (Agtr1) expression and was sensitive to P2ry6 modulators. Proximity ligation assay and super-resolution microscopy showed closer localization of Agtr1 and P2ry6 at/near the membrane of BPH mice. This proximal association was reduced in BPN mice, suggesting a functional role for Agtr1-P2ry6 complexes in the hypertensive phenotype. Intriguingly, BPN mice were resistant to AgtII-induced HT and showed reduced P2ry6 expression in VSMCs. Altogether, results suggest that increased functional coupling between P2ry6 and Agtr1 may contribute to enhanced vascular reactivity during HT. In this regard, blocking P2ry6 could be a potential pharmacological strategy to treat HT.

Introduction

Essential hypertension (HT) is the most relevant modifiable contributing factor to the burden of coronary artery disease, stroke, and chronic kidney disease, and it is one of the main causes of morbidity and mortality worldwide.[1,2] In most cases, the etiology is unknown[3] and the clinical management combines lifestyle modifications and several pharmacological approaches.[4] These treatments are often unsuccessful, bringing to the forefront the need for an improved knowledge of the molecular and cellular mechanisms related to the control of blood pressure (BP).[5–7]

One pathophysiological mechanism key to the development of HT is the increase in vascular resistance. This is caused mainly by the reduction in the diameter of small resistance arteries due to the increased contraction of vascular smooth muscle cells (VSMC).[8] The contractile response of VSMC depends on the pressure within the vessel (myogenic response[9]), as well as the delicate balance of vasoconstrictor and vasodilator pathways. Many animal models have been used to define the molecular hallmarks associated with HT.[10] Genetic models are the most extensively used. Among them, the spontaneously hypertensive rats (SHR) have become the reference rodent model of human essential HT. More recently, the hypertensive Schlager mouse (BPH) has been described as a polygenetic model of HT.[11] Since the BPH strain and the normotensive control strain (BPN) have been obtained by random selection of breeding partners from the same population, both strains share the same genetic background, improving the comparisons of the pathophysiological changes related to the hypertensive phenotype. This is a clear advantage against the SHR model, which does not seem to share the genetic background of the Wistar-Kyoto rats used as controls.[12] BPH mice are increasingly being used as an experimental model of HT, and some reports describe a relevant role for the sympathetic system in the model.[13,14] However, relatively few articles have focused on the vascular pathophysiology of BPH, and our knowledge of vascular mechanisms driving the increase in vascular resistance in this mouse model is still scarce. Our laboratory has performed a thorough characterization of the differential expression of ion channels in VSMC of BPH mesenteric arteries[15–20] disclosing several differences relevant to understanding the hypercontractility of BPH vessels. Endothelial dysfunction and extensive differential vascular remodeling of the aorta, femoral, and mesenteric arteries have also been recently reported.[21]

In this study, aiming to find relevant differences in the function of VSMC from BPH that could contribute to define the hypertensive phenotype, we have compared gene expression in VSMC from BPN and BPH mesenteric arteries using Affymetrix GeneChip arrays. Among the more conspicuous changes observed were differences in the expression of purinergic receptors, particularly P2ry6. The involvement of purinergic signaling in vascular pathophysiology is well established,[22] and P2ry6 receptors have been associated with HT through the formation of heterodimers with the angiotensin II receptors.[23,24] In this work, we have characterized the purinergic responses in BPN and BPH mice testing the functional crosstalk with the angiotensin II mediated responses. Results may point to P2ry6 as a potential therapeutic target to treat HT.

Material and Methods

Colonies of BPN/3 J, BPH/2 J, and C57BL/6 J mice (Jackson Laboratories, Bar Harbor, ME, USA) were housed in the animal facility of the School of Medicine of Valladolid, under temperature-controlled conditions (21°C) and with unlimited access to water and food. Mice were fed with a standard rodent chow diet (SD; Research Diets, #D12450J). All animal protocols were approved

by the Institutional Care and Use Committee of the University of Valladolid and are in accordance with the European Community guiding principles in the care and use of animals.

In Vivo Procedures

BP was monitored using the CODA setup (Kent Scientific Corporation, Torrintgon, CT, USA). Animals were restrained in a holder and acclimated to 32°C-35°C on a heat platform for 15 min before data collection. Measurements were performed on awake mice at the same time each day to reduce animal stress and ensure reliable data. Each session consisted of 40 cycles of an inflation step to a maximum occlusion pressure of 250 mmHg, followed by a deflation step of 15 s. The first 5 cycles were considered part of the training and were not included in the analysis. This protocol was performed for 4-6 consecutive days and the first 2 days were not used for determinations.

A group of adult male BPN and BPH were subjected to chronic treatment with losartan (0.6 mg mL^{-1}) for 6 weeks in drinking water, changing the bottles every 2 days.

Surgical Procedures

Mice were anesthetized by inhalation of isoflurane administered with a SomnoSuite® Low-Flow Anesthesia System (Kent Scientific) at a dose of 2% for induction and 1%-2% for maintenance of anesthesia at low flow rates of 500 mL min^{-1} and 45 mL min^{-1}, respectively. Mice were anaesthetized and an AgtII minipump (model 1007D, Alzet, 800 ng kg^{-1} min^{-1}) was inserted in the intrascapular region under the skin in a group of BPN and C57 mice. In this set of experiments, control BP measurements were performed at least 3 days before the protocol and experimental data were obtained 3, 7, and 14 days after surgery. For the rest of experiments, mice were decapitated after anesthesia. After killing, ~1 mL trunk blood samples were collected in tubes containing ethylenediaminetetraacetic acid (EDTA) and centrifuged at 1500 g for 15 min at 4°C. The plasma was stored at −80°C for subsequent ELISA assays. The animals were then placed in the supine position, and a surgical incision was made to gain access to the abdominal cavity. The mesenteric arcade was removed and kept in a Sylgard®-coated plate containing ice-cold (4°C) aerated (95% O$_2$-5% CO$_2$) solution containing (in mM): NaCl, 120; KCl, 4.2; MgCl$_2$·6H$_2$O, 1.2; NaCHO$_3$, 25; KH$_2$PO$_4$, 0.6; glucose, 11; CaCl$_2$, 0.01; pH 7.4 (adjusted with NaOH). Segments of second and third-order mesenteric arteries were carefully dissected out and cleaned from adipose, connective, and endothelial tissues. Arteries were either frozen (−80°C) for ulterior RNA extraction, cut into small segments for cell isolation or mounted in a pressure or wire myograph.

Isolation of Vascular Smooth Muscle Cells

VSMCs were dissociated as previously described.[25] Briefly, the protocol used a physiological magnesium solution (MgPSS) with the following constituents (in mM): NaCl, 140; KCl, 5; MgCl$_2$·6H$_2$O, 2; Hepes, 10; glucose, 10; pH 7.4 (adjusted with NaOH). Segments of second and third-order mesenteric arteries were placed in MgPSS containing 1 mg mL^{-1} papain (3119, Worthington, Lakewood, NJ, USA) and 1 mg mL^{-1} 1,4-dithioerythritol (D9163, Sigma) and incubated in it for 9 min at 37°C. This was followed by a second 9 min incubation in MgPSS with 1.77 mg mL^{-1} collagenase H (C8051, Sigma), 0.5 mg mL^{-1} Elastase (2292, Worthington), and 1 mg mL^{-1} Trypsin inhibitor (T9003, Sigma). After 3 washes in ice-cold MgPSS buffer solution, mechanical trituration was performed with a wide-necked glass pipette to obtain fresh VSMCs. The enzymatic solutions were prepared daily. Arterial myocytes were stored in dissection buffer at 4°C until further use.

Arrays and PCR Validation

Total RNA from arteries was isolated with MELT^{TM} Total RNA Isolation System Kit (Ambion, Inc., Austin, TX, USA) as previously described.[17] Five to six second and third-order mesenteric arteries of five mice were employed for each determination. The quality of total RNA was assessed with the Agilent Bioanlayzer and samples were prepared for hybrization to the Affymetrix GeneChip® MG-430 2.0 Array according to Affymetrix instructions, in the Genomic Service of the CIC (Salamanca, Spain). After DNAse I (Ambion, Life Technologies) treatment, 500-750 ng of RNA was used for the reverse transcription reaction (2.5 u/μL MuLvRT, 1 u/μL RNAse inhibitor, 2.5 μM random hexamers, 1× PCR buffer, 5 mM MgCl$_2$, and 4 mM mixed dNTPs, Applied Biosystems) at 42°C for 60 min, to get cDNA. Differential gene expression was analyzed with the "LIMMA" R package (3.52.1) with log FC $\geq$ 0.5 and adjusted P value < 0.05.[26,27] To elucidate the potential biological mechanisms of genes related to the hypertensive phenotype, enrichment analyses were performed using the "gprofiler2" R package (0.2.2), using the gSCS correction method, the expressed genes as background genes and Gene Ontology (GO), KEGG, Reactome (REAC), WikiPathways (WP), TRANSFAC (TF), and CORUM as data sources [28,29]

Real-time PCR validation of selected genes was carried out using TaqMan Low Density Arrays (Applied Biosystems, Life Technologies) and an ABI Prism 7900HT sequence detection system (Applied Biosystems) at the Genomic Service of the CNIC (Madrid, Spain). Data were analyzed with the threshold cycle (Ct) relative quantification method ($\Delta\Delta$Ct).[30] Expression data were normalized by the level of ribosomal RNA 18S transcript. The relative abundance of the genes was calculated from $2^{(-\Delta Ct)}$, where $\Delta Ct = Ct_{Channel}-Ct_{18S}$. Differences between BPN and BPH samples were calculated from $2^{(-\Delta\Delta Ct)}$, where $\Delta\Delta Ct=\Delta Ct_{BPH}-\Delta Ct_{BPN}$. When changes are expressed as $\log 2^{(-\Delta\Delta Ct)}$, positive values mean a higher expression in BPH mice, whilst negative values mean lower expression, compared with BPN mice.

Myography Measurements

Segments of second and third order mesenteric arteries were mounted in either a pressure or a wire myograph (Danish Myo Technology, Aarhus, Denmark).

For pressure-myography the arteries were cannulated between two borosilicate glass pipettes and fixed with nylon filaments at both ends. Then, the artery segment was air bubbled to remove endothelia tissue and filled with Physiological Saline Solution-PSS (120 mM NaCl, 2.5 mM CaCl$_2$, 1.17 mM MgSO$_4$, 5 mM KCl, 1.18 mM Na$_2$HPO$_4$, 25 mM NaHCO$_3$, 1 mM EDTA, 10 mM Glucose, pH 7.4 adjusted with 5% CO$_2$-95% air), which was maintained throughout all the experiment. The arteries were pressurized to 70 mmHg in PSS solution and incubated at 37°C for at least 20 min to equilibrate before starting the measurements. Data of external diameter were collected with a CCD camera placed in an inverted DMT microscope and was analyzed using MyoView software. At the end of each experiment, vessels were superfused with a solution containing 10 μM nifedipine to determine maximal vessel diameter upon relaxation. Dose-response curves of chemical agents were calculated with the formula $100 \times (D - D_{Stimulus})/(D_{Nif} - D_{Stimulus})$.

Wire-myography experiments were performed on 2 mm sections of second and third-order mesenteric arteries that were mounted on two 25 μm tungsten wires. The myograph baths were filled with PSS, maintained at 37°C, and aerated with 95% O_2/5% CO_2. Arteries were left to rest for a period of ~15 min, and subsequently subjected to a passive force normalization procedure.[31] Changes in tension were recorded using LabChart (AD Instruments, Hastings, UK). Arteries were constricted with 120 mM K^+ and treated with 10 μM acetylcholine to confirm the lack of endothelium. To normalize the data, contraction is usually expressed as a percentage of high K^+ vasoconstriction. However, in the present study, we have used absolute values of tension, because large differences between BPN and BPH were observed (3.07 ± 0.18 mN in BPH versus 1.62 ± 0.16 mN in BPN, $P < 0.001$).

Dose-response curves were fitted to Hill functions with one (a) or two ($a + b$) components:

$$Tension = \left\{ \frac{(T_{max})_a \cdot [Agonist]^{n_a}}{(EC_{50})_a^{n_a} + [Agonist]^{n_a}} \right\}_a + \left\{ \frac{(T_{max})_b \cdot [Agonist]^{n_b}}{(EC_{50})_b^{n_b} + [Agonist]^{n_b}} \right\}_b.$$

Proximity Ligation Assays

A Duolink In Situ Proximity Ligation Assay (PLA) Kit (Sigma-Aldrich) was used to detect complexes of P2ry6 and Agtr1 receptors in VSMCs from BPN and BPH lines. Freshly isolated cells were plated out and allowed to adhere for 1 h on 25-mm-diameter glass coverslips at RT. Cells were fixed with 3% glyoxal for 20 min, then quenched with 100 mM glycine for 15 min, and then washed twice with the PBS protocol (×1). The permeabilization step was performed with 0.1% Triton X-100 for 20 min and then cells were blocked with 50% Odyssey Blocking Solution (LI-COR Bioscience) for 1 h at RT. A 2-h incubation at 4°C with a specific combination of the 2 primary antibodies was performed in 0.01% Odyssey + 0.05% Triton X-100 PBS solution. The working factor dilution of the primary antibodies was rabbit anti-P2ry6 (1:800; Genetex, GTX16829) and goat anti-Agtr1 (1:800; Novus Biologicals NB100-57073). Samples with only one primary antibody were used as negative controls. After exposure of the primary antibody, cells were washed with Duolink buffer A (×2 for 5 min). Oligonucleotide-conjugated secondary antibodies (PLA probes: anti-goat MINUS and anti-rabbit PLUS) were incubated at 37°C for 1 h. Last, cells were washed 3 times with buffer A and then a ligase enzyme solution (1 U/μL, dilution 1:40) was incubated at 37°C for 30 min. After washing 3 times with PBS, amplification was performed by polymerase enzyme (10 U/μL, dilution 1:80 in Duolink In site detection reagents orange) at 37°C incubation for 100 min. After washing twice with buffer solution B for 10 min and once for 1 min with ultrapure water, samples were completely dried and mounted on a slide with Duolink mounting medium and stored protected from light at 4°C until visualization by confocal microscopy. An Olympus FV1000 confocal microscope with a ×60 oil immersion objective (NA, 1.4) was used to visualize the fluorescence signals. Images were acquired in different optical planes (z-axis step = 0.5 μm) using Olympus Fluoview v1.4 software. For each sample, a single intensity projection image from the combined image stack was used for analysis of the number of spots per cell area (μm²). The analysis was performed using NIH Image J v1.51 open software.

Super-Resolution Microscopy

Mesenteric arterial myocytes were isolated from BPN or BPH mice. Cells were plated onto circular coverslips (#1.5, catalog no. 64-0715, Warner Instruments, USA). Cells were fixed using a glyoxal fixing solution for 20 min at room temperature and subsequently quenched for an additional 15 min in 100 mM Glycine (catalog # G8898, Sigma-Aldrich). Permeabilization and epitope blocking was performed by incubating the cells with a blocking solution containing 50% fish serum blocking buffer (catalog # 37527, ThermoFisher Scientific, USA) and 0.5% Triton X-100 (Sigma-Adrich) in PBS for 1 h at room temperature. The cells were incubated with the primary antibodies goat anti-Agtr1 (1:100, catalog # NB100-57073, Novus Biologicals, USA) and rabbit anti-P2ry6 (1:100, catalog # GTX16829, GeneTex, USA) diluted in antibody incubation block solution at a 1:4 ratio of fish serum blocking buffer: PBS and 0.5% of Triton X-100 for 2 h at room temperature. After 5× washes with PBS, 15 min per wash cycle, the secondary antibody Alexa-Flour 647 donkey anti-goat (1:1 000, catalog # A21447, ThermoFisher Scientific, USA) was diluted in blocking solution and added to the cells for 1 h at room temperature. After 5× washes with PBS, 15 min per wash cycle, the secondary antibody Alexa-Fluor 568 goat anti-rabbit (1:1 000, catalog # A11011, ThermoFisher Scientific, USA) was added to the cells for another hour at room temperature followed by another 5 × 15 min wash. Cells were stored at 4°C until imaging was performed.

Super-resolution imaging of Agtr1 and P2ry6 was carried out using coverslips mounted on a round cavity microscope slide (catalog # BR475505, Sigma, USA). ONI Bcubed buffers A + B (100:1, catalog # BCA0017, ONI) were added to the round cavity center, followed by the placement of the coverslips with the cells upside down. Localization maps images were acquired using a microscope coupled to a 100× Olympus oil-immersion UPlanApo TIRF 1.5 NA objective. Samples were imaged sequentially using 640 nm (1000 mW) and 561 nm (500 mW) lasers, with emission collected using the corresponding filter cubes. Images were acquired at 100 Hz with 10 ms of exposure rate. 30 000 images were acquired to construct a pointillist localization map image. Rendered images were filtered using the following parameter range values: photon count (600-10 000 000), σ_{locx} (0-25 nm), σ_{locy} (0-25 nm), σ_X (100-400), σ_Y (100-400), and P-value (0.6-1.0). Image acquisition was done using the ONI NimOS v.1.18.3 software.

Biophysical characterization of the Agtr1 and P2ry6 clusters, including the intermolecular distance between the two receptors, was performed using pair and cross-correlation algorithms written in MatLab (R2023a, Mathworks, Natick, MA, USA) as in.[32–34] Autocorrelation (g(r)) and cross-correlation (c(r)) functions were obtained from regions of interest (ROIs) with an area of 6.25 μm². Special care was taken to avoid placing the ROIs on visible "holes" in the cell image in order to minimize artifacts arising from membrane topography. Parameters such as cluster area, cluster density ($\Psi^{cluster}$), molecules per cluster, and intermolecular distance were obtained by fitting the correlation functions with exponential models as in.[32–34]

Enzyme-Linked Immunosorbent Assays

A competitive in vitro enzyme-linked immunosorbent assay (ELISA) was performed to determine the plasmatic concentration of AgII (RayBio®, catalog # EIA-ANGII) and aldosterone (Invitrogen, catalog #EIAALD), whereas the concentration of
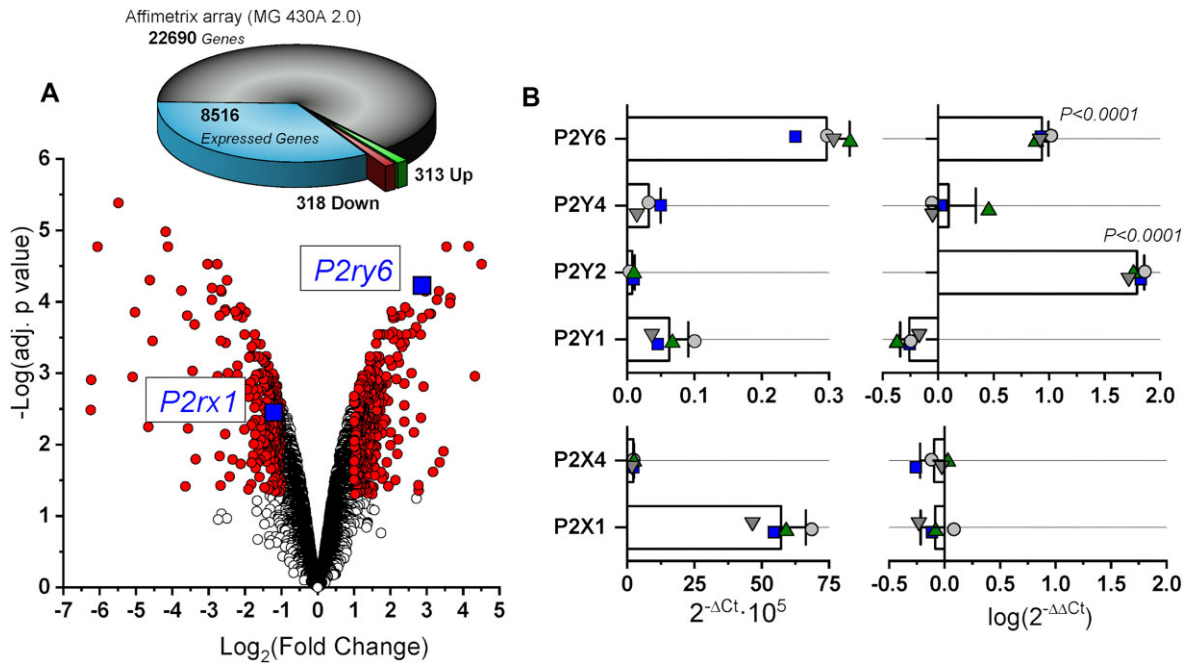
Figure 1. Purinergic receptor expression in BPN and BPH mice. (A) Vulcano plot representing the *P* value versus the fold change of the 8516 genes expressed in endothelium-denuded arteries from BPN and BPH mice, considering BPN expression as control. Filled dots correspond to the 631 genes with changes considered significant (*P* < 0.05 and changes bigger than 2-fold above or below control). The list of all genes with *P* values and expression data are provided as supplemental material. Squares correspond to the P2 receptors found in the array. (B) mRNA expression levels of P2 receptors studied by qPCR. Expression levels are normalized with respect to rRNA18S. Relative abundance was plotted on the left graphs an expressed as $2^{-\Delta Ct} \cdot 10^5$ where $\Delta Ct = Ct_{receptor} - Ct_{18s}$. The right graphs show differences in P2 receptors expression in BPH arteries (using BPN expression levels as calibrator, where $\Delta\Delta Ct = \Delta Ct_{BPH} - \Delta Ct_{BPN}$), and represented in log scale, so that negative values mean decreased expression and positive values increased expression. Each bar is the mean ± SD of 4 samples, and each sample results from pooling 30 mesenteric arteries from 5 different mice (6 arteries per mouse), so that a total of 20 animals have been used for each group. Significance was calculated by a one-way ANOVA followed by Tukey's post-hoc test. Only *P* values < 0.05 are shown in the figures.

renin (Invitrogen, catalog #EMREN1) was assessed using a sandwich ELISA assay, following manufacturing instructions.

Statistics

Plots and Graphs were created with Origin Pro 2024 (Origin-Lab Corp., Northampton, MA, USA). Data processing and analysis was carried out with Microsoft Excel, and statistical analysis was performed using Origin Pro or R-Studio. Data are represented as the mean ± standard deviation (SD). Exemplary images and traces were selected to represent group means. To account for potential variability in sample preparation, animals, ambiance conditions, and other factors, datasets were obtained from arteries obtained from at least 3 different mice. The number of replicates and mice used are included in figure legends.

For comparisons between more than 2 groups, ANOVA analysis followed by Tukey's test was used when the distribution was normal and the variances were equal. Alternatively, Kruskal-Wallis analysis followed by Dunn's test was used. Shapiro-Wilk test and Levene test were used to test normality and homogeneity of variances, respectively. In some cases, statistical significance was determined using hierarchical "nested" analyses and linear mixed effects models that take into consideration the number of mice used as well as the arteries collected from each mouse. This analysis was carried out in R using the lme4 package.[35] Details of the analysis performed in each case are provided in the figure legends. The replicates from each mouse are color-and shape-coded in the figures.

Results

Gene Differential Expression in Mesenteric Arteries From BPN and BPH Mice

To study the molecular signatures determining the hypertensive phenotype in vascular smooth muscle cells (VSMCs) of mesenteric arteries, we compared the basal gene expression profiles of BPH versus BPN arteries using Affymetrix GeneChip® Mouse Genome 430A 2.0 Array. A file with all expressed genes is provided in the supplemental material section. In BPH mice, 313 genes were more than 2-fold upregulated, and 318 were more than 2-fold downregulated compared to BPN samples (adjusted *P* values < 0.05). These 631 genes represent 7.4% of the total genes expressed in VSMCs. GO enrichment analysis based on biological process (BP) revealed more than 600 significant GO terms when the whole annotated mouse genome was used as background (a selection of the more relevant ones is in the supplemental material section). However, when only the expressed genes were used as background, there was not any GO enrichment. Nevertheless, several relevant genes related to smooth muscle contractility were differentially expressed. Interestingly, P2Y and P2X purinergic receptor expression seem to be different in an opposite way (Figure 1A), and whilst P2ry6 was among the genes more upregulated (7.3-fold), P2rx1 expression was downregulated (2.3-fold). Microarray data were verified by performing real time PCR analysis. Although similar results were obtained for P2ry6 (ie, 7.1-fold higher in BPH), no differences in P2rx1 expression were found between BPN and BPH samples (Figure 1B). qPCR data also show that P2X receptors expression
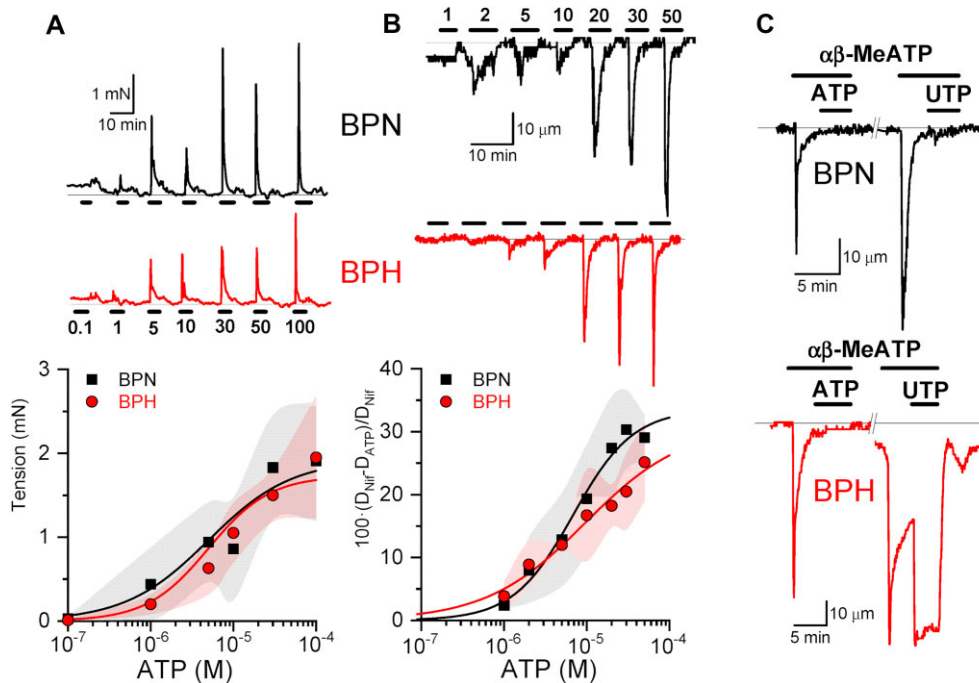
Figure 2. Vasoconstrictor responses elicited by ATP in BPN and BPH mesenteric arteries. Representative traces and dose-response curves with mean ± SD data obtained with ATP in a wire (A) or a pressure (B) myograph. In all cases, arteries were allowed to relax between pulses of different doses of ATP. SD values are represented as shadows. An average of 2-16 arteries from 2-4 mice were used in each group. Solid traces represent the fit of a Hill function to the data (see methods). F-test comparison between the fits were not significant. (C) Representative traces showing two pulses of 5 μM $\alpha\beta$-methylene-ATP applied to BPN (upper traces) and BPH (bottom traces) arteries mounted in a pressure myograph. ATP (50 μM) or UTP (50 μM) pulses were also applied as indicated in the figure.

is considerably higher than P2Y receptors (~200 times), as previously described in human vascular smooth muscle,[36] and that P2ry6 is the more abundant P2Y receptor both in BPN and in BPH, despite the upregulation of P2ry2 in BPH arteries.

Contractile Responses to Purinergic Stimulation in BPN and BPH Mesenteric Arteries

The functional consequences of the differential expression of purinergic receptors were tested by measuring the contractile responses elicited on endothelial-denuded mesenteric arteries from BPN and BPH mice. Dose-response curves obtained with ATP in wire (Figure 2A) and pressure myograph (Figure 2B) show no differences between BPN and BPH arteries. ATP responses were kinetically almost identical to those obtained with α,β-methylene ATP (α,β-MeATP), a selective P2XR agonist. ATP failed to produce any effect following the decay of the response triggered by α,β-MeATP (Figure 2C), strongly indicating that ATP responses were mediated by P2X receptors and ruling out a significant functional role for P2ry2, which is also activated by ATP. Strikingly, UTP, which is a P2YR agonist, induced a strong contraction in BPH but not BPN arteries in the presence of α,β-MeATP (Figure 2C). The distinct response to UTP in BPN and BPH arteries was tested carrying out dose-response curves (Figure 3). Under the pressure myograph (Figure 3A), the EC$_{50}$ for UTP was ~3 μM in BPH, while BPN arteries were mostly unresponsive. Similar results were obtained in the wire myograph (Figure 3B), where UTP responses could be fitted to Hill functions with EC$_{50}$ of 424 μM (black line) and 3.7 μM (red line) for BPN and BPH arteries, respectively. UTP responses in BPH arteries were slightly better fitted with a two-binding site model (gray line) with T$_{max}$ and EC$_{50}$ for the high (blue) and low (green) affinity components depicted in the box plots.

Contractile Responses to UTP Are Mediated Mainly By P2ry6

Since P2ry2 and P2ry6 were upregulated in BPH, we tested the relative contribution of both receptors to the UTP contractile response (Figure 4). UDP of 10 μM and 10 μM PSB0474 (selective agonists for P2ry6 [37,38]) induced responses in the pressure myograph that were ~70% and ~45%, respectively, of the response elicited by similar concentration of UTP. UTPγS (a selective agonist of P2ry2/4) of 10 μM elicited a response that was ~27% of that of UTP. In all cases, responses in BPN were minimal. Since we have not carried out a full dose-response curve characterization for all agonists, it is not possible to precisely define the amount of the response mediated by each receptor, although results strongly suggest that the UTP responses are mainly mediated by P2ry6. The responses to UTP and UDP are also highly sensitive to MRS2578, a specific P2ry6 blocker, although surprisingly only when the inhibitor is applied after the agonist (Figure 4B).

AgtII Responses Are Higher in BPH Arteries

Since P2ry6 receptors have been described to heterodimerize with AgtII receptors, and this cross-talk may contribute to promote HT,[23] we decided to characterize the AgtII effects on vascular reactivity in the BPN and BPH mesenteric arteries. Dose-response curves obtained with AgtII in BPN and BPH arteries are shown in Figure 5A. As AgtII responses were fast and transient, dose-response curves were obtained by applying only one pulse per artery and averaging at least 4 arteries at each concentration. BPN response was well fitted to a Hill function with an EC$_{50}$ of 17.3 ± 0.4 nM (black line), while BPH response deviated from a typical Hill function (red line, EC$_{50}$ 3.7 ± 2.7 nM) exhibiting a peak response at 100 nM. BPH arteries are more sensitive to
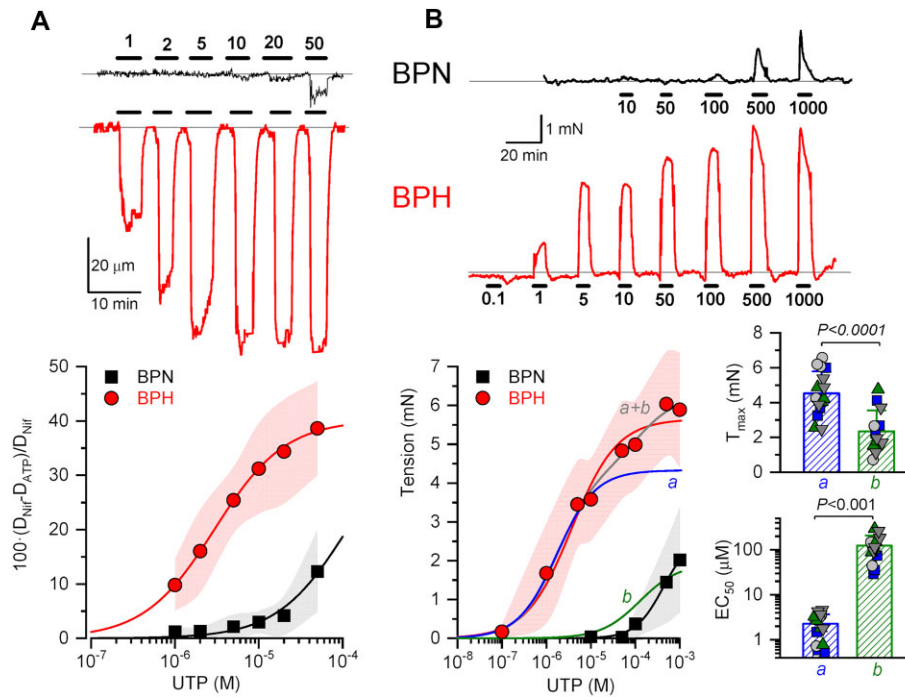
Figure 3. Vasoconstrictor responses elicited by UTP in BPN and BPH mesenteric arteries. Representative traces and dose-response curves with mean ± SD data obtained with UTP in a pressure (A) or a wire (B) myograph. In all cases, arteries were allowed to relax between pulses of different doses of UTP. SD values are represented as shadows. An average of 4-16 arteries in each group from 2-8 mice. Black traces correspond to BPN mice, and red to BPH mice. Curves were fitted to a Hill function (see methods). The P values for the F-test comparison of fits between BPN and BPH data are < 0.0001 both, for pressure and wire myography. The dose-response curve obtained in BPH with the wire myograph is also fitted to a Hill function with two (gray) binding sites (blue and green). Fitting parameters (T_{max} and EC_{50}) of the two binding sites model (a + b) are represented in the bar plots. Significance was calculated by a nested one-way ANOVA followed by Tukey's post-hoc test.
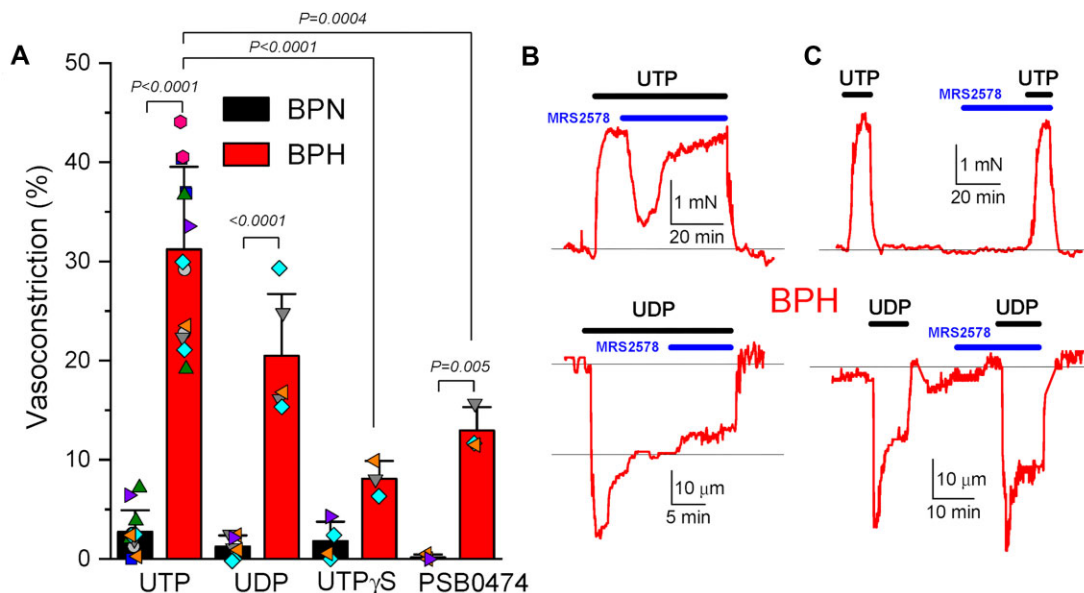
Figure 4. Effects of P2Y agonists and blockers on vascular tone in BPN and BPH mesenteric arteries. (A) Contractile responses obtained in the pressure myograph in BPN (black) and BPH (red) arteries with the indicated agonists. In all cases, the concentration was 10 μM. An average of 3-13 arteries in each group from a total of 6 BPH and 7 BPN mice. P values are obtained with a nested 2-way ANOVA followed by Tukey´s post-hoc test. (B) Effect of 10 μM MRS2578, a specific blocker of P2ry6, on contractile responses elicited by UTP or UDP in BPH arteries, determined by wire (upper traces) or pressure (bottom traces) myography. (C) As in B but using a two-pulse protocol and applying the blocker before the second pulse.

Figure 5. AgtII responses in BPN and BPH arteries. (A) Dose-response curve of AgtII obtained in the wire myograph with BPN (black) and BPH (red) arteries. SD values are represented as shadows. Solid lines are fits to a Hill function. The *P* value for the F-test comparison of fits between BPN and BPH data is 0.007. For al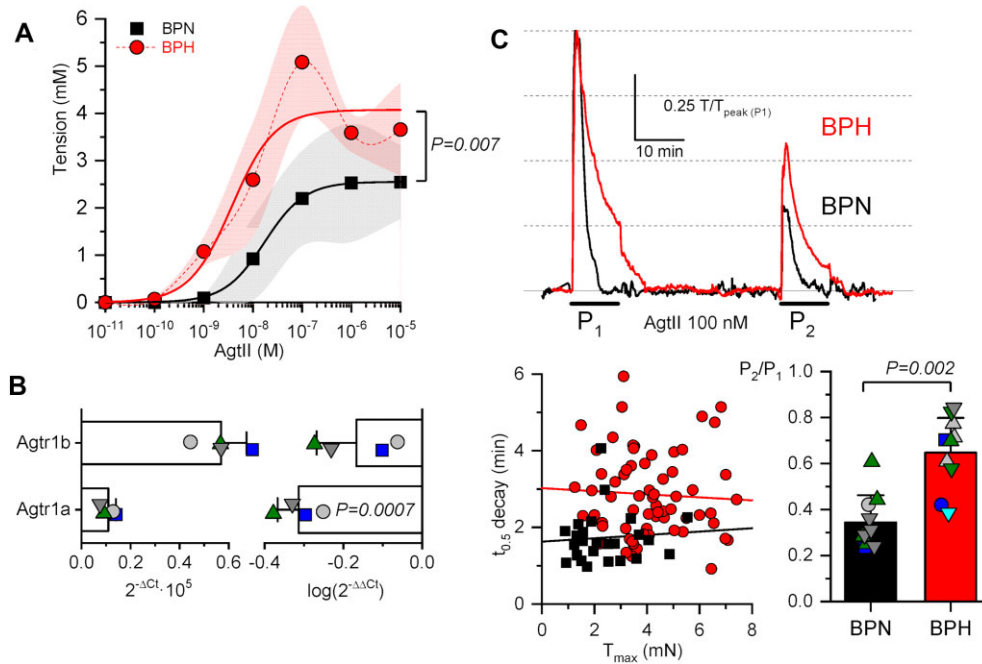l measurements, AgtII was applied only once at a single dose in every tested artery (an average of 2-45 arteries in each group from 2-10 mice). (B) Relative abundance of Agtr1 receptors studied by qPCR expressed as $2^{-\Delta Ct} \cdot 10^5$ where $\Delta Ct = Ct_{receptor} - Ct_{18s}$. Bars in the right side shows fold changes in expression expressed as $\log(2^{-\Delta\Delta Ct})$ as in Figure 1B, where $\Delta\Delta Ct = \Delta Ct_{BPH} - \Delta Ct_{BPN}$. Each bar is the mean ± SD of 4 samples, and each sample results from pooling 30 mesenteric arteries from 5 different mice (6 arteries per mouse). (C) Sample traces of two 10 min pulses of AgtII applied with a separation of 30 min in BPN (black) and BPH (red) arteries. Traces are normalized to the peak tension of the first pulse. The time course of decay, estimated as the time needed to get a tension half of the T_{peak} ($t_{0.5}$) in the first pulse is plotted against T_{peak} in the scatter plot in the bottom left. Each dot represent data obtained in single arteries from 10 BPN (black squares) and 28 BPH (red circles) mice. The desensitization at 30 min, estimated as the ratio P_2/P_1 is shown in the box plot in the bottom right (an average of 10 arteries from 4 BPN mice and 11 arteries from 5 BPH mice). Statistical comparisons were made using a nested one-way ANOVA followed by Tukey's post-hoc test.

AgtII, and that effect seems to be unrelated to differences in the expression of AgtII receptors (Figure 5B). Both isoforms of AgtII receptor 1(Agtr1a and Agtr1b) are expressed in mesenteric arteries, and both are less expressed in BPH mice (0.48- and 0.7-fold) despite having a higher AgtII response. Responses to AgtII in BPH mice are also kinetically different from those in BPN. Figure 5C shows representative traces obtained in BPN (black) and BPH (red) arteries with a protocol of two 10 min AgtII pulses separated by 30 min. Both traces are normalized with respect to the peak tension at the first pulse. AgtII responses are transient, and the decay measured as the time needed to get a tension half of the T_{peak} ($t_{0.5}$), was plotted against T_{peak} in the scatter plot in the bottom left of Figure 5C. This parameter was independent of T_{peak} (at least for $T_{peak} > 1$ mN) and was significantly slower in BPH ($t_{0.5} = 2.85 \pm 1.09$ min in BPH versus 1.73 ± 0.67 min in BPN, P < 0.0001). Desensitization was estimated as the ratio P_2/P_1 (box plot of Figure 5C) and was significantly smaller (P_2/P_1 closer to 1) in BPH arteries (0.65 ± 0.15 in BPH versus 0.34 ± 0.11 in BPN).

Agtr1 and P2ry6 Are Closer in VSMCs From BPH Mesenteric Arteries

Since BPH changes in AgtII responses and Agtr1 expression do not correlate, we hypothesize that a higher formation of Agtr1-P2ry6 heterodimers in BPH VSMCs potentiates the AgtII responses. To check if the formation of these heterodimers is possible, we investigated how close the receptors are to

each other at/near the membrane using PLA and superresolution microscopy (Figure 6). Figure 6A shows representative PLA images of VSMCs cells from BPN and BPH arteries labeled with antibodies against Agtr1 and P2ry6. The number of puncta (normalized by the cell size) obtained in several cells are shown in the same figure. On average, there is a significant increase of puncta in the BPH cells (0.05 ± 0.03 puncta/μm^2 in BPN versus 0.15 ± 0.05 puncta/μm^2 in BPH), suggesting that both receptors are closer in the hypertensive cells. We confirmed this finding analyzing the arrangement of both receptors in the plasma membrane of VSMCs using point-localization super-resolution imaging. Figure 6B shows pointillist single-molecule images obtained after labeling BPN and BPH VSMCs with antibodies against Agtr1 (red) and P2ry6 (green). The areas of interest (squares) labeled in the merge images are zoomed in at bottom. Analysis of the images (Figure 6C) revealed significant changes for the Agtr1 clusters in BPH cells: Cluster area was smaller (6319 ± 3842 in BPN versus 2864 ± 1800 in BPH), cluster density ($\psi^{cluster}$) was higher (4.7 ± 3.5 in BPN versus 39.9 ± 12.45 in BPH) and the number of molecules per cluster increased $\sim$7-fold (1.47 ± 1.60 in BPN versus 10.2 ± 9.9 in BPH). However, P2ry6 clusters had similar areas in BPN and BPH, whilst cluster density (7.0 ± 4.5 in BPN versus 25.2 ± 11.4 in BPH) and the number of molecules per cluster (0.4 ± 0.9 in BPN versus 10.8 ± 12.3 in BPH) were significantly higher in BPH. Interestingly, the distribution of intermolecular distances between Agtr1 and P2ry6 was quite different between BPN and BPH (Figure 6D). The means of both distributions were quite similar (145.9 in BPN versus 125.8 in BPH), but medians (144.2 nm in BPN versus 70.8 nm in BPH) and skewness (0.4 in BPN versus 2.6 in BPH) were quite different.
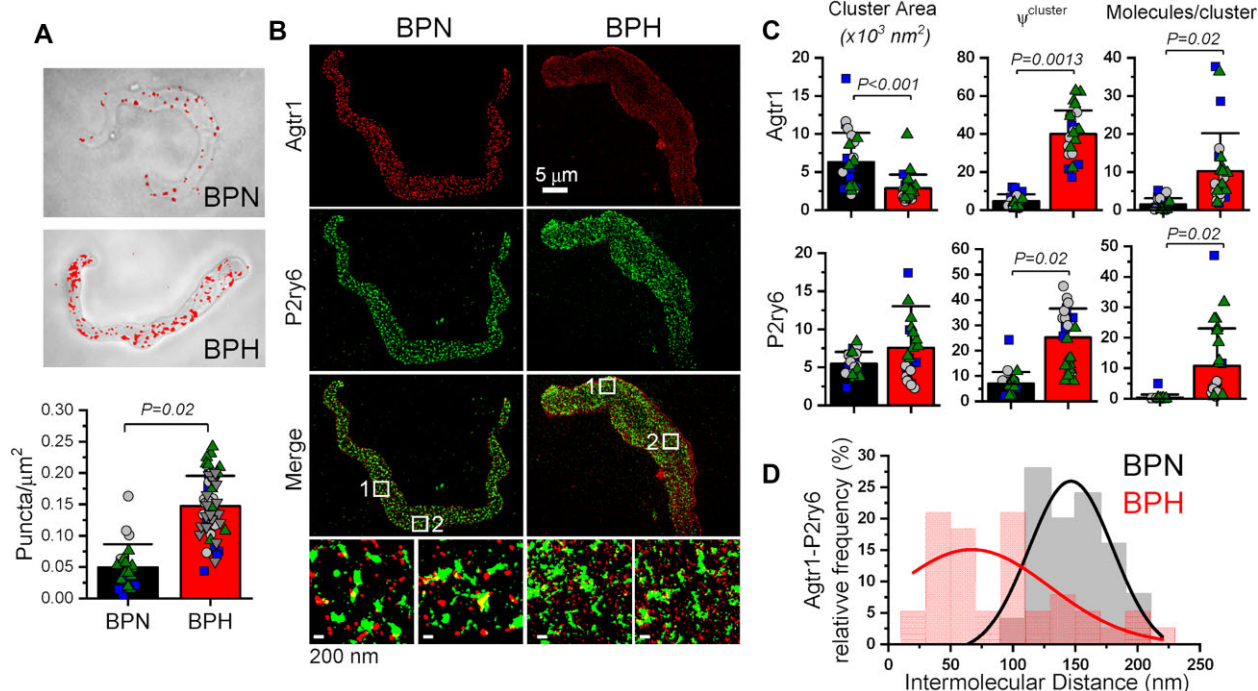
Figure 6. Colocalization of P2ry6 and Agtr1 receptors in the plasma membrane of VSMCs from BPN and BPH mesenterica arteries. (A) PLA sample images of single BPN and BPH VSMCs obtained with antibodies against Agtr1 and P2ry6. Fluorescence (red) and bright field (gray) images are superimposed. The number of puncta normalized by the cell size obtained in several cells are shown as bar graphs in the bottom panel. Data are obtained in 22 cells from 3 BPN mice and 50 cells form 4 BPH mice. (B) Typical pointillist single-molecule images of Agtr1 and P2ry6 receptors obtained in a BPN (left) and a BPH (right) VSMCs. The regions of interest marked in the merged images are magnified and depicted at the bottom of the corresponding images. (C) Bar graphs of cluster areas, cluster density ($\psi^{cluster}$) and molecules/cluster obtained upon analysis of the pointillist single-molecule images of Agtr1 and P2ry6 receptors obtained in BPN (gray) and BPH (red). Each bar contains data from 25 cells obtained either from 3 BPN or 3 BPH mice. (D) Distribution of intermolecular distances (nm) between Agtr1 and P2ry6 obtained in BPN (gray bins) and BPH (red bins). An average of 25 cells in each group from three independent experiments. Significance was calculated by a nested one-way ANOVA followed by Tukey's post-hoc test.

Whilst the BPN distribution is quite symmetric, the BPH distribution is heavily right skewed, with a significant proportion of Agtr1 and P2ry6 located at much closer distances in BPH than in BPN.

BPH AgtII Contractile Responses Are Modulated By P2ry6 Activity

The closer location of Agtr1 and P2ry6 receptors in BPH VSMCs suggested a differential interaction between them in BPH and BPN VSMCs. We tested that interaction, exploring the effect of blocking P2ry6 receptors on the AgtII contractile response. Figure 7A shows representative traces of 10 min pulses of 100 nM AgtII obtained in BPN (left) and BPH (right) arteries with and without applying MRS2578 at the time indicated by the arrows. Traces are normalized to T_{peak} to visualize the effect of the blocker on the time course of the decay of the AgtII response (gray versus red trace). P2ry6 blockade had no effect on BPN but significantly speed up the decay of AgtII response on BPH arteries, strongly suggesting an interaction between P2ry6 and Agtr1 receptors. The decay of AgtII responses was evaluated as the percentage of T_{peak} remaining at the end of the 10 min pulse or as the time interval between points where tension was 50% and 75% of the T_{peak}. Those results are depicted in Figure 7B. Following the same rationale, P2ry6 simulation should have an effect opposite to MRS2578, slowing down the decay of AgtII responses. To test that hypothesis, we carried out a two-pulse protocol in pairs of BPH arteries in the wire myograph as shown in Figure 7C. Red traces were obtained in one artery stimulated by two pulses of 10 μM UDP (P_1 and P_2) separated by 60 min, whilst gray traces

were obtained in the second artery with a similar protocol but applying a 50 min. prepulse of 100 nM AgtII before the second pulse. Traces from both arteries are normalized to the T_{peak} of P1. The ratio of peak tension amplitudes of pulses P_1 and P_2 in both arteries are shown in the bar graph to the right. Figure 7D illustrates the results obtained in other pair of BPH arteries applying an identical protocol but using 10 μM Phenylephrine (PHE) instead of UDP. Figure 7E shows bar graphs measuring the time course of the decay of the AgtII response as the percentage of the AgtII maximal response remaining after 50 min when PHE (8.5 ± 2.9%) or UDP (24.8 ± 10.8%) were used as the stimuli for P_1 and P2. For the sake of comparison, the time course of the decay of single 60 min. pulses of AgtII 100 nM, applied without any previous stimuli (traces not shown, 10.8 ± 7.1%) is also included in Figure 7E. Although previous stimulation with PHE (P_1) has no effect on AgtII decay (no significant differences with single pulses of AgtII), UDP almost doubles the contractile response of AgtII remaining at 50 min, as expected if P2yr6 receptor activation potentiates AgtII response slowing down its decay. Unexpectedly, it seems that Agtr1 activation has no effect on P2ry6 responses since P_2/P_1 ratio for UDP was identical independently of applying the AgtII prepulse before P_2 (Figure 7C, bars graph).

Plasma AgtII Concentration Is Smaller in BPH Mice

The higher responses to AgtII of BPH arteries suggested a relevant role of the renin/AgtII system in the genesis of the hypertensive phenotype. To explore that hypothesis, we tested the contribution of AgtII to BP control in BPN and BPH mice, measuring the effect of losartan added to the drinking water (0.6 mg
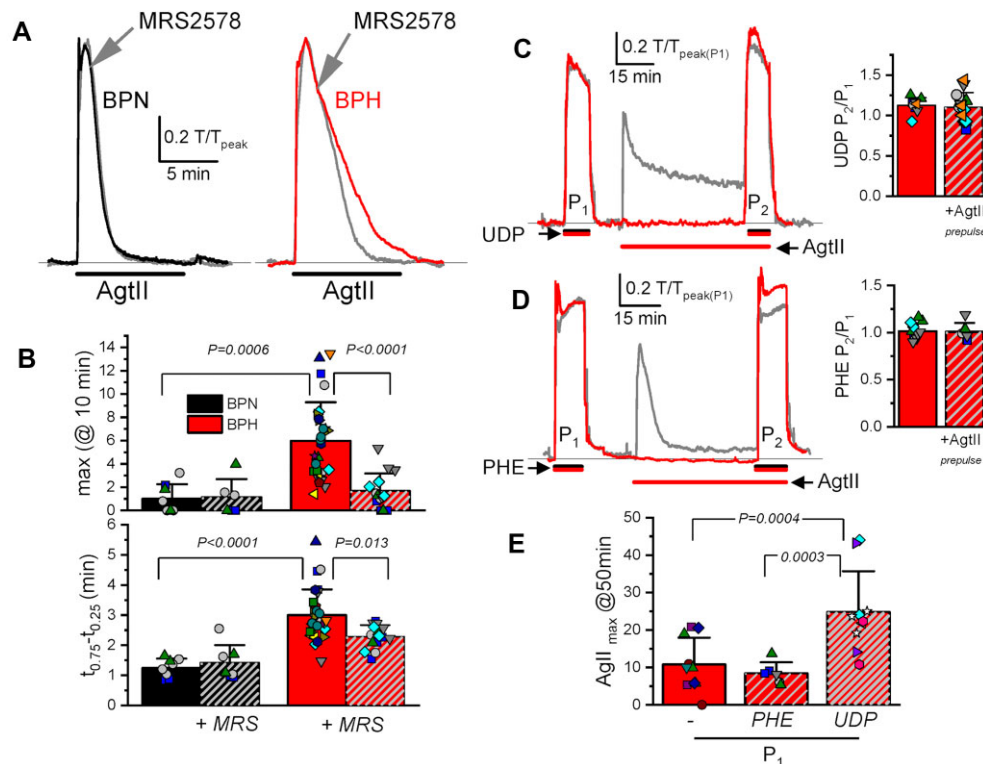
Figure 7. Functional interaction of Agtr1 and P2ry6 receptors. (A) Sample traces of 100 nM AgtII pulses obtained in a BPN (left) and in a BPH (right) artery. Superimposed to those traces are identical pulses (gray) obtained in a different artery applying MRS2578 at the time indicated. In all cases, traces are normalized to the maximal response to appreciate the kinetic effects of MRS2578. (B) Percentage of peak tension remaining after 10 min stimulation (upper graph bars) and the time needed to decrease tension from a 25% to a 75% of the peak (lower graph bars) obtained in several experiments like those shown in A. Black bars depict data from BPN and red from BPH arteries. Bar graphs represent the average of 8 arteries from 3 BPN mice and 28 arteries from 15 BPH mice. A nested 2-way ANOVA followed by Tukey's post-hoc test was used to estimate significance. (C) Sample trace obtained in one BPH artery stimulated in the wire myograph by two pulses of 10 μM UDP (P_1 and P_2) separated by 60 min (red). Superimposed (gray) trace was obtained in another artery with a similar protocol but applying a 50 min. prepulse of 100 nM AgtII before P_2. Traces are normalized to $P_1 T_{peak}$. The ratio of peak tension amplitudes of pulses P_1 and P_2 in several experiments (9-13 arteries from 6 mice) are shown in the bar graph to the right. (D) As C but using 10 μM PHE as stimulus in P_1 and P_2. Bar graphs represent the average of 7-10 arteries from 8 mice. (E) Bar graphs showing the decay of the AgtII response obtained in 6-10 arteries from 9 BPH mice with protocols like those depicted in C and D. Decay is estimated as the percentage of the peak tension remaining immediately before applying P_2. The bar labeled as P_1(-) represents measurements of decay in single 50 min isolated pulses of AgtII (10 arteries from 5 different mice). Nested one-way ANOVA and Tukey's test were applied for comparisons.

mL^{-1}). The obtained changes in mean, diastolic, and systolic BP measured over 6 weeks are depicted in Figure 8A. Losartan had a big effect on BP in both strains, but unexpectedly, the effect was larger in BPN mice, suggesting a more relevant role of the Renin/AgtII system in the normotensive mice. We explored this possibility by measuring basal levels of renin, AgtII and aldosterone in blood samples obtained from BPN, BPH, and C57 mice (Figure 8B). As expected, due to the reported bigger sympathetic drive of BPH mice,[14] renin levels were ∼2-fold higher in that strain (21.6 ± 3.5 ng/mL in BPH versus 10.9 ± 0.6 ng/mL in BPN) but surprisingly, AgtII was ∼2-fold higher in BPN (2.3 ± 0.5 pg/mL in BPH versus 4.2 ± 1.4 pg/mL in BPN) whilst aldosterone levels were not significantly different (0.4 ± 0.1 ng/mL in BPH versus 0.38 ± 0.13 ng/mL in BPN). Interestingly, C57 mice levels of renin, AgtII (Figure 8B) and BP values (Figure 8C) were intermediate between those of BPN and BPH mice, disclosing an inverse relationship between AgtII plasma levels and BP. In this sense, it is interesting to note that a key difference between BPN and C57 is the sensitivity to P2ry6 activation since UTP responses in C57 arteries are almost identical to those recorded in BPH (EC$_{50}$ = 2.5 ± 0.32 μM and T$_{max}$ = 5.4 ± 0.14 mN, Figure 8C). Moreover, BPN mice, in addition to having lower BP values with higher levels of plasma AgtII, were insensitive to the exogenous administration of AgtII through osmotic minipumps for 2 weeks. This

protocol produced the expected results when carried out in C57 mice (Figure 8D).

Discussion

Experimental models of HT have been developed over the years and have filled some of the gaps in our knowledge of the regulation of BP. Advantages and disadvantages are present in each model and depending on the selection, different aspects of the physiopathology of the disease can be highlighted. In this study, we used VSMCs of mesenteric arteries from the Schlager BPH mice to explore the molecular determinants of the hypertensive phenotype. Differences in gene expression in mesenteric vessels free of endothelium from BPN and BPH mice were explored with the Affymetrix GeneChip® Mouse Genome 430A 2.0 Array. This kind of array is less sensitive than the Low Density Taqman arrays we have used extensively in our laboratory to study the differential expression of ion channels,[15–19] but have the advantage of exploring the expression of 22 690 genes. Among them, we found 8516 significantly expressed either in BPN or BPH arteries. In BPH mice, 313 genes were more than 2-fold up regulated and 318 were more than 2-fold down regulated in comparison to BPN mice.
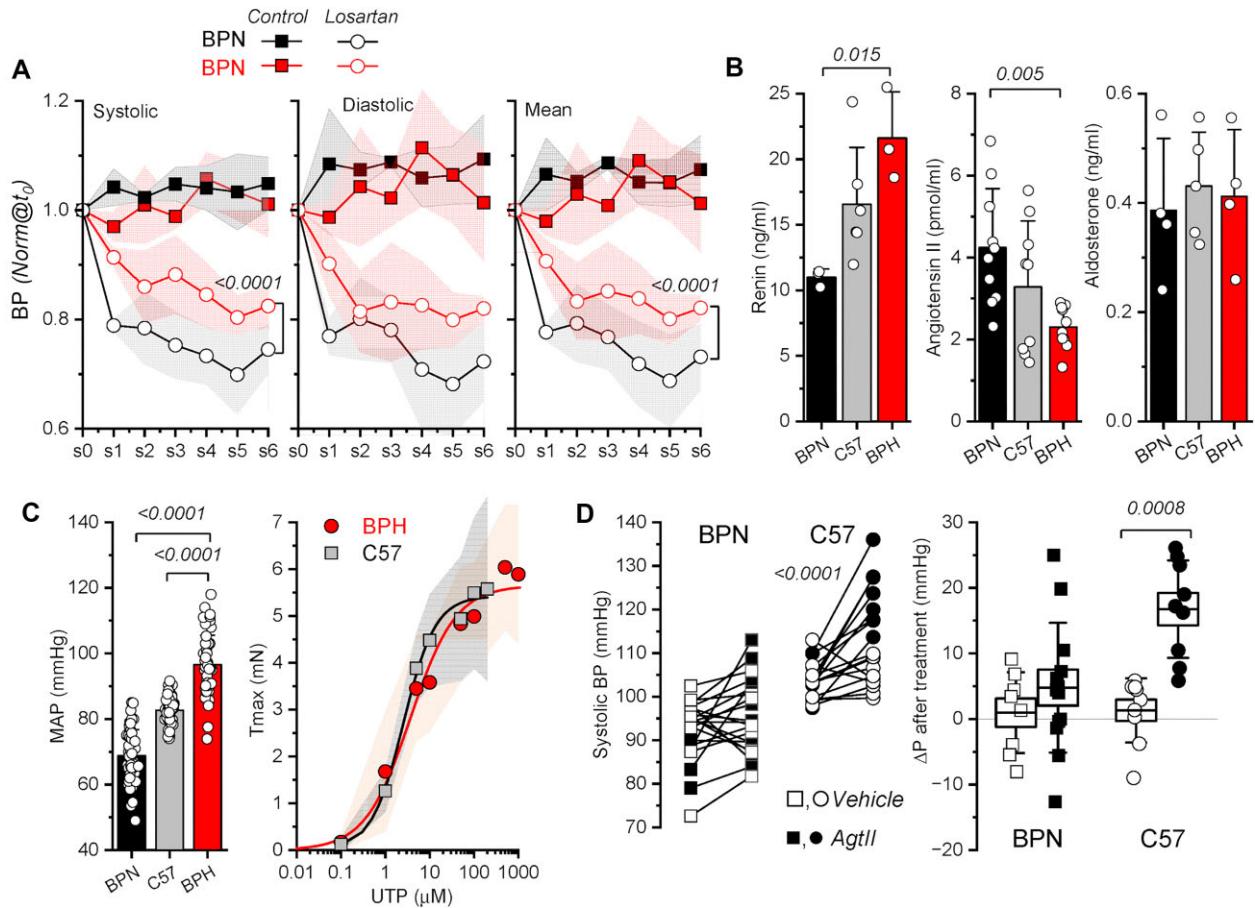
Figure 8. Renin-Angiotensin system in BPN and BPH mice. (A) Effect of chronic treatment with losartan (0.6 mg mL^{-1} in drinking water) during 6 weeks on mean, diastolic, and systolic BP of BPN and BPH mice. Data are represented a percentage of change of the BP measured before starting the treatment. Data are mean ± SD of 3 BPN and 5 BPH mice for the control and 4 BPN and 6 BPH mice for the experimental condition. SD values are represented as shadows. Significance was calculated by a 2-way ANOVA of repeated measurements followed by Tukey´s post-hoc test. (B) Renin, AgtII, and Aldosterone levels measured in resting conditions from plasma samples obtained from BPN, BPH, and C57. Each bar represent mean ± SD data collected from 3-10 samples obtained from 3-10 mice in each case. Significance was calculated by one-way ANOVA followed by Tukey's post-hoc test. (C) Comparison of the MAP (an average of 48-52 mice in each group) and the dose-response curves for UTP of C57 and BPH mice (an average of 5-16 arteries from 2-8 mice). Groups were compared using 1-way ANOVA followed by Tukey's post-hoc test. (D) Effect of 2 weeks exogenous administration of AgtII trough osmotic minipumps on systolic BP of BPN and C57 mice. Left, before-after plot showing the effect of AgtII (black symbols, 13 BPN and 9 C57 mice) or vehicle (open symbols, 8 BPN and 9 C57 mice). Significance was calculated by a 2-way ANOVA of repeated measurements followed by Tukey's post-hoc test. Right, box blots showing the average effects measuring the differences in BP before and after the AgtII treatment. Open symbols, vehicle; black symbols, AgtII. One-way ANOVA followed by Tukey's post-hoc test were applied for comparisons.

GO enrichment analysis is a statistical approach to determine whether certain GO terms are significantly overrepresented in a given set of genes or proteins compared to what would be expected by chance. GO terms are typically categorized into Biological Process (BP, a series of molecular events or functional pathways), Molecular Function (MF, the activity of gene products) or Cellular Component (CC, where gene products are active in the cell). GO enrichment analysis based on BP, the more relevant category for this study, revealed more than 600 significant GO BP terms when the completely annotated mouse genome was used as background. The long list of GO terms obtained would imply that all those pathways are related to the hypertensive phenotype. However, when only the 8516 expressed genes were used as background, there was not any GO enrichment, suggesting that the enrichment obtained when the full genome was used as background in the analysis has to do with the enrichment of the vascular smooth muscle phenotype, not with HT (see[39] for an interesting discussion on the subject). Although similar arrays have been used to test differences

in expression between BPN and BPH in aorta, brain, liver, heart, and kidney,[11,40–45] this is the first study focusing on VSMCs. If we consider the polygenic nature of HT,[6] it is not surprising that the 630 genes we found differentially expressed pervade so many different pathways, making it quite difficult to interpret the real meaning of the changes. In the end, it is necessary to test the functional relevance of those changes, and that requires focusing on the characterization of every relevant change. In this work, we decided to characterize the purinergic system since P2ry6 appears in the top list of the upregulated genes in BPH mice (Figure 1).

We have tested receptor expression and functional responses mediated by P2x and P2y receptors. Whilst P2rx expression and function is almost identical in BPN and BPH arteries, there is a remarkable difference in P2ry responses. As described previously in other preparations,[36] we found that the expression levels of ionotropic P2x receptors are significantly higher than those of P2y receptors. It is important to note that, despite the similar expression of P2x receptors in BPN and BPH mice, their

elevated expression may become crucial for vessel function under conditions where purine nucleotide levels change significantly, such as in HT. Among P2ry1/2/4/6, P2ry6 is the more abundant receptor both in BPN (75% P2ry6, 15% P2ry1, 8% P2ry4) and in BPH (80% P2ry6, 18% P2ry2) arteries, although its expression is ∼7 fold higher in BPH arteries. Functionally, BPN arteries barely respond to P2y agonists (Figure 3) whilst BPH arteries exhibit a strong response mainly mediated by P2ry6 receptors. UDP of 10 μM and 10 μM PSB0474 (selective agonists for P2ry6) induced similar responses in the pressure myograph (if we consider that PSB0474 potency is half of that of UDP[46]), higher than those elicited by 10 μM UTPγS (a selective agonist of P2ry2/4). Surprisingly, despite a significant expression of P2y2/4 receptors, ATP did not elicit any response mediated by those receptors, as evidenced by the lack of any remaining ATP-induced contraction in the presence of α,β-MeATP (see figure 2C).

Paracrine release of nucleotides into the bloodstream occurs under many physiological and pathological conditions. Uridine nucleotides measurements are scarce, but the presence of uridine in micromolar concentrations in normal human plasma [47] suggests that discrete release of UTP may be physiologically relevant. Although the increased expression of P2ry6 has been demonstrated in several pathological contexts,[48,49] few studies have been conducted in HT. In endothelial cells, P2ry6 upregulation was associated with vascular inflammation.[50] In cardiomyocytes, P2ry6 upregulation was associated with pressure overload and cardiac fibrosis.[51] In VSMCs, P2ry6 was reported to be the dominant purinergic component involved in responses mediated by extracellular nucleotides, as UTP or UDP. These responses were abrogated in mesenteric arteries in KO P2ry6 mice.[52] In the context of HT, it has been recently demonstrated that P2ry6 heterodimerize with Agtr1, and that those heterodimers are required to promote the AgtII-induced HT, since P2ry6 antagonists suppress the AgtII effect.[23] GPCR oligomerization has been described in several pathological contexts,[53–55] although not many papers have been focused on HT. Apart from Nishimura´s work, a functional interaction between Agtr1 and the bradykinin type 2 receptor was found in human placental biopsies from pregnancies with preeclampsia,[56] and Agtr1 homodimers have been described in monocytes from patients with HT.[57]

AgtII responses are larger and desensitized slowly in BPH arteries despite a smaller expression of Agtr1 (Figure 5). These larger responses have also been recently reported in intact BPH mesenteric arteries,[21] although a comparison between BPN and BPH in that work was carried out normalizing the responses to contractions elicited in high K+. We hypothesized that those differences could be related to the existence of functional P2ry6-Agtr1 heterodimers in the VSMCs from BPH arteries.[23] PLA and super-resolution microscopy reveal a higher probability of finding P2ry6 and Agtr1 located close enough to form those heterodimers in BPH VSMCs. Although we have not demonstrated the physical association with biochemical approaches, we have evidenced the functional association by exploring the effects of blocking or activating P2ry6 on the responses elicited by AgtII (Figure 7). Responses to AgtII decay faster when P2ry6 receptors are bound to the specific inhibitor MRS2578 and the time course of decay is significantly slower when P2ry6 are previously activated with UDP. These effects are only significant in arteries from BPH mice, and strongly suggest that P2ry6-Agtr1 interaction is responsible of the kinetic differences between BPN and BPH arteries. The functional interaction seems to be unidirectional since P2ry6 responses are not affected by the previous activation of Agtr1 (Figure 7C). P2ry6 effects on responses

mediated by Agtr1 can be a consequence of attenuated Agtr1 phosphorylation, a reduction in Agtr1 endocytosis and/or increased Agtr1 recycling, as previously described.[58,59] In addition, P2ry6 receptors induce Gαq11-mediated signaling pathways, while Agtr1 receptors activate both the Gαq11 and Gα12-13 pathway, so that heterodimers can promote crosstalk between the two signaling pathways and could result in the coupling of P2ry6 receptors to other G proteins. GPCR signaling does not result from sequential activation of a linear pathway, but rather from the complex interactions of multiple, branched signaling networks. In this context, heterodimerization of GPCRs can generate signaling phenotypes that may be interpreted as signaling pathway crosstalk, as it is the case of some well characterized examples of receptor crosstalk in the cardiovascular system.[60,61]

Notwithstanding the larger responses to AgtII in BPH arteries, chronic administration of losartan has a larger effect in BPN mice. This fact correlates well with the lower levels of AgtII we found in BPH mice (Figure 8A, B). The study of the renin/AgtII system is complex and contradictory results can be found in the literature.[62] An earliest work reported equal plasma renin levels between BPN and BPH.[63] However, in a more recent work, a higher plasma renin level was found in the SHR genetic model.[64] The higher renin secretion could be explained by the increased sympathetic activity through renal β1-ARs described in both patients and hypertensive animal models.[65] This greater amount of plasma renin was consistent with our results. However, the increased renin levels did not promote increased AgII production. Of note, other studies have described similar results. For example, Uddin and Harris-Nelson also found a higher concentration of renin and a lower concentration of AgtI in the submandibular gland of the BPH model.[66] The authors proposed a faster metabolization of AgtI in BPH as a possible explanation for this controversy. AgtII is hydrolyzed by ACE2 to angiotensin 1-7, which acts as a vasodilator. Several works have measured ACE2 in both tissue and plasma of HT animal models and patients. ACE2 inhibition was implicated in HT development, while ACE2 potentiation was associated with HT resistance.[67] Increased ACE2 activity in BPH could represent a compensatory mechanism to prevent further increases in BP by lowering AgtII levels. We have not explored this hypothesis further, but ACE2 is expressed both in endothelial and VSMCs of many vascular beds,[68] and in the Affymetrix arrays, ACE2 was downregulated in BPH ∼7 fold (see Supplemental Data).

Altogether, our data suggest that renin/AgtII system overstimulation is not implicated in the development of high BP in the BPH model. Similar results have been reported by other groups, studying the renin/AgtII system in the BPH model.[13] This work suggested that while the renin/AgtII is an important contributor to BP, it has little or no involvement in the development of HT in BPH mice. In contrast to our results, they found no differences in the hypotensive effect of losartan between BPN and BPH. This slight discrepancy could be due to the shorter treatment period used in this study. In addition, another potential difference could be the interpretation of the data. These authors reported no changes in BP levels after two weeks losartan treatment, comparing the absolute values; mean blood pressure (MAP) was reduced 23 mmHg in BPN and 25 mmHg in BPH mice. However, considering that MAP is significantly higher in BPH, changes in absolute terms most likely reflect a smaller decrease of BP in BPH mice when expressed as % of change compared to time 0, as we did in our analysis. In fact, they acknowledge this effect in a more recent work in which they explored the contribution of the sympathetic and renin/AgtII system in these mice during the active (night) and inactive (light)

period, as they conclude that there is a decreased % contribution of the renin/AgtII to BP in BPH during light[69] as we found here. In any case, the role of the brain renin-angiotensin system has not been studied in this model. It is known that intracerebral AgtII regulates sympathetic activity,[70] so that the presence of P2ry6/Agtr1 heteromers in the brain could contribute to the increased sympathetic influence on blood pressure in BPH mice.

The upregulation of P2ry6 in BPH seems to be a clear hallmark of the hypertensive phenotype in this model of HT. However, the activity of P2y dependent pathways does not correlate with the phenotype, since UTP responses elicited in mesenteric arteries from C57 mice, a strain considered as control in many experimental setups, are quite similar to those obtained in BPH (Figure 8C). In any case, BP, renin and AgtII levels of C57 mice are between values obtained on BPN and BPH (Figure 8B and C). These results drove us to focus in the BPN strain. Although robust P2ry6 responses do not correlate with high BP, the lack of responses seems to favor a low BP phenotype. Therefore, the purinergic system could represent a promoter of the hypertensive phenotype in the proper pathophysiological context. In this regard, after 2-week infusion of AgtII in BPN and C57 strains, only C57 showed a significant increase in BP (Figure 8D). We hypothesize that the lack of functional P2ry6 in BPN mice contributes to generate the resistance to develop AgtII-dependent HT. In other words, P2ry6-Agtr1 heterodimers are necessary for this AgtII effect. This role of P2ry6 is supported by data from the literature, since P2ry6-KO mice showed decreased BP levels after AgtII infusion-dependent HT.[23] Nevertheless, our data certainly do not prove causality, and other effects of P2ry6 such as those described in endothelium should be considered to elucidate the final role of these receptors in vivo. Additional experimental approaches directed to demonstrate the effects on BP of the blockade of P2yr6 or its genetic manipulation will be required to give support to the hypothesis. If proven true, this receptor could become a promising target for the treatment of HT.[24]

Acknowledgements

Author Contributions

Nuria Daghbouche-Rubio (Data curation, Investigation, Methodology, Validation, Writing – review & editing), Inés Álvarez-Miguel (Data curation, Formal analysis, Investigation, Validation, Writing – review & editing), Victor Alejandro Flores (Data curation, Formal analysis, Investigation, Methodology), Jorge Rojo-Mencía (Data curation, Formal analysis, Investigation), Manuel Navedo (Conceptualization, Formal analysis, Methodology, Resources, Writing – review & editing), Madeleine Nieves-Citrón (Conceptualization, Data curation, Funding acquisition, Investigation, Methodology, Resources, Writing – review & editing), Pilar Cidad (Data curation, Formal analysis, Investigation, Methodology, Validation, Visualization, Writing – review & editing), M. Teresa Pérez-García (Conceptualization, Data curation, Formal analysis, Funding acquisition, Investigation, Resources, Supervision, Validation, Writing – review & editing), and José R. López-López (Conceptualization, Data curation, Formal analysis, Funding acquisition, Investigation, Methodology, Project administration, Resources, Software, Validation, Writing – original draft)

Supplementary Material

Supplementary material is available at the *APS Function* online.

Funding

Conflict of Interest

M.T.P.G. holds the position of Editorial Board Member for *Function* and is blinded from reviewing or making decisions for the manuscript.

Data Availability

The data underlying this article are available in the article and in its online supplementary material. Raw data will be shared on reasonable request to the corresponding author.

References

1. Oparil S, Acelajado MC, Bakris GL, et al. Hypertension. *Nat Rev Dis Primers* 2018;**4**(1):18014.
2. World Health Organization. The Global Health Observtvatory. Blood pressure/hypertension. https://www.who.int/data/gho/indicator-metadata-registry/imr-details/3155. Accessed 24 July 2023.
3. Messerli FH, Williams B, Ritz E. Essential hypertension. *Lancet North Am Ed* 2007;**370**(9587):591–603.
4. Heidari B, Avenatti E, Nasir K. Pharmacotherapy for essential hypertension: a brief review. *Methodist Debakey Cardiovasc J* 2022;**18**(5):5–16.
5. Padmanabhan S, Joe B. Towards precision medicine for hypertension: a review of genomic, epigenomic, and microbiomic effects on blood pressure in experimental rat models and humans. *Physiol Rev* 2017;**97**(4):1469–1528.
6. Padmanabhan S, Dominiczak AF. Genomics of hypertension: the road to precision medicine. *Nat Rev Cardiol* 2021;**18**(4):235–250.
7. Harrison DG, Coffman TM, Wilcox CS. Pathophysiology of hypertension: the Mosaic Theory and beyond. *Circ Res* 2021;**128**(7):847–863.
8. Touyz RM, Alves-Lopes R, Rios FJ, et al. Vascular smooth muscle contraction in hypertension. *Cardiovasc Res* 2018;**114**(4):529–539.
9. Davis MJ, Hill MA. Signaling mechanisms underlying the vascular myogenic response. *Physiol Rev* 1999;**79**(2):387–423.
10. Lerman LO, Kurtz TW, Touyz RM, et al. Animal Models of Hypertension: a scientific statement from the American Heart Association. Krantz DS, Baum A, Singer JE, Singer JL, eds. *Hypertension* 2019;**73**(6):155–197.
11. Zhu Y, Zhuo J, Li C, Wang Q, Liu X, Ye L. Regulatory network analysis of hypertension and hypotension microarray data from mouse model. *Clin Exp Hypertens* 2018;**40**(7):631–636.
12. Zhang-James Y, Middleton FA, Faraone SV. Genetic architecture of Wistar-Kyoto rat and spontaneously hypertensive rat substrains from different sources. *Physiol Genomics* 2013;**45**(13):528–538.

13. Palma-Rigo K, Jackson KL, Davern PJ, Nguyen-Huu TP, Elghozi JL, Head GA. Renin-angiotensin and sympathetic nervous system contribution to high blood pressure in Schlager mice. *J Hypertens* 2011;**29**(11):2156–2166.

14. Davern PJ, Nguyen-Huu TP, La Greca L, Abdelkader A, Head GA. Role of the sympathetic nervous system in schlager genetically hypertensive mice. *Hypertension* 2009;**54**(4):852–859.

15. Tajada S, Cidad P, Moreno-Domínguez A, Pérez-García MTT, López-López JRJR. High blood pressure associates with the remodelling of inward rectifier K+ channels in mice mesenteric vascular smooth muscle cells. *J Physiol* 2012;**590**(23):6075–6091.

16. Tajada S, Cidad P, Colinas O, Santana LF, López-López JR, Pérez-García MT. Down-regulation of CaV1.2 channels during hypertension: how fewer CaV1.2 channels allow more Ca2+ into hypertensive arterial smooth muscle. *J Physiol* 2013;**591**(24):6175–6191.

17. Moreno-Domínguez A, Cidad P, Miguel-Velado E, López-López JR, Pérez-García MT. De novo expression of Kv6.3 contributes to changes in vascular smooth muscle cell excitability in a hypertensive mice strain. *J Physiol* 2009;**587**(3):625–640.

18. Álvarez-Miguel I, Cidad P, Pérez-García MT, López-López JR. Differences in TRPC3 and TRPC6 channels assembly in mesenteric vascular smooth muscle cells in essential hypertension. *J Physiol* 2017;**595**(5):1497–1513.

19. Cidad P, Moreno-Domínguez A, Novensá L, et al. Characterization of ion channels involved in the proliferative response of femoral artery smooth muscle cells. *ATVB* 2010;**30**(6):1203–1211.

20. Daghbouche-Rubio N, López-López JR, Pérez-García MT, Cidad P. Vascular smooth muscle ion channels in essential hypertension. *Front Physiol* 2022;**13**(September):1016175.

21. Jelinic M, Jackson KL, O'Sullivan K, et al. Endothelium-dependent relaxation is impaired in Schlager hypertensive (BPH/2 J) mice by region-specific mechanisms in conductance and resistance arteries. *Life Sci* 2023;**320**(February):121542.

22. Burnstock G. Purinergic signaling in the cardiovascular system. *Circ Res* 2017;**120**(1):207–228.

23. Nishimura A, Sunggip C, Tozaki-Saitoh H, et al. Purinergic P2Y 6 receptors heterodimerize with angiotensin AT1 receptors to promote angiotensin II–induced hypertension. *Sci Signal* 2016;**9**(411):1–13.

24. Sunggip C, Nishimura A, Shimoda K, Numaga-Tomita T, Tsuda M, Nishida M. Purinergic P2Y(6) receptors: a new therapeutic target of age-dependent hypertension. *Pharmacol Res* 2017;**120**:June:51–59.

25. Prada MP, Syed AU, Reddy GR, et al. AKAP5 complex facilitates purinergic modulation of vascular L-type Ca2+ channel CaV1.2. *Nat Commun* 2020;**11**(1):1–14.

26. Ritchie ME, Phipson B, Wu D, et al. limma powers differential expression analyses for RNA-sequencing and microarray studies. *Nucleic Acids Res* 2015;**43**(7):e47–e47.

27. Phipson B, Lee S, Majewski IJ, Alexander WS, Smyth GK. Robust hyperparameter estimation protects against hypervariable genes and improves power to detect differential expression. *Ann Appl Stat* 2016;**10**(2):946–963.

28. Raudvere U, Kolberg L, Kuzmin I, et al. g:profiler: a web server for functional enrichment analysis and conversions of gene lists (2019 update). *Nucleic Acids Res* 2019;**47**(W1):W191–W198.

29. Kolberg L, Raudvere U, Kuzmin I, Vilo J, Peterson H. gprofiler2—an R package for gene list functional enrichment analysis and namespace conversion toolset g:profiler. *F1000Res* 2020;**9**:Jul 15:709.

30. Livak KJ, Schmittgen TD. Analysis of relative gene expression data using real-time quantitative PCR and the 2^(-△△CT) method. *Methods* 2001;**25**(4):402–408.

31. Mulvany MJ, Halpern W. Contractile properties of small arterial resistance vessels in spontaneously hypertensive and normotensive rats. *Circ Res* 1977;**41**(1):19–26.

32. Sengupta P, Jovanovic-Talisman T, Lippincott-Schwartz J. Quantifying spatial organization in point-localization superresolution images using pair correlation analysis. *Nat Protoc* 2013;**8**(2):345–354.

33. Veatch SL, Machta BB, Shelby SA, Chiang EN, Holowka DA, Baird BA. Correlation functions quantify super-resolution images and estimate apparent clustering due to overcounting. *PLoS One* 2012;**7**(2):e31457.

34. Sengupta P, Jovanovic-Talisman T, Skoko D, Renz M, Veatch SL, Lippincott-Schwartz J. Probing protein heterogeneity in the plasma membrane using PALM and pair correlation analysis. *Nat Methods* 2011;**8**(11):969–975.

35. Bates D, Mächler M, Bolker BM, Walker SC. Fitting linear mixed-effects models using lme4. *J Stat Soft* 2015;**67**(1):1–48.

36. Wang L, Karlsson L, Moses S, et al. P2 Receptor expression profiles in Human vascular smooth muscle and endothelial cells. *J Cardiovasc Pharmacol* 2002;**40**(6):841–853.

37. von Kügelgen I. Pharmacological profiles of cloned mammalian P2Y-receptor subtypes. *Pharmacol Ther* 2006;**110**(3):415–432.

38. Vallon V, Unwin R, Inscho EW, Leipziger J, Kishore BK. Extracellular nucleotides and P2 receptors in renal function. *Physiol Rev* 2020;**100**(1):211–269.

39. Timmons JA, Szkop KJ, Gallagher IJ. Multiple sources of bias confound functional enrichment analysis of global -omics data. *Genome Biol* 2015;**16**(1):15–17.

40. Guo S, Deng W, Xing C, Zhou Y, Ning M, Lo EH. Effects of aging, hypertension and diabetes on the mouse brain and heart vasculomes. *Neurobiol Dis* 2019;**126**(June):117–123.

41. Nelson JW, Ferdaus MZ, McCormick JA, et al. Endothelial transcriptomics reveals activation of fibrosis-related pathways in hypertension. *Physiol Genomics* 2018;**50**(2):104–116.

42. Chiu CL, Jackson KL, Hearn NL, Steiner N, Head GA, Lind JM. Identification of genes with altered expression in male and female Schlager hypertensive mice. *BMC Med Genet* 2014;**15**(1):101.

43. Friese RS, Ye C, Nievergelt CM, et al. Integrated computational and experimental analysis of the neuroendocrine transcriptome in genetic hypertension identifies novel control points for the cardiometabolic syndrome. *Circ Cardiovasc Genet* 2012;**5**(4):430–440.

44. Marques FZ, Campain AE, Davern PJ, Yang YHJ, Head GA, Morris BJ. Global identification of the genes and pathways differentially expressed in hypothalamus in early and established neurogenic hypertension. *Physiol Genomics* 2011;**43**(12):766–771.

45. Puig O, Wang IM, Cheng P, et al. Transcriptome profiling and network analysis of genetically hypertensive mice identifies potential pharmacological targets of hypertension. *Physiol Genomics* 2010;**42A**(1):24–32.

46. Rafehi M, Müller CE. Tools and drugs for uracil nucleotide-activated P2Y receptors. *Pharmacol Ther* 2018;**190**(October):24–80.

47. Yamamoto T, Koyama H, Kurajoh M, Shoji T, Tsutsumi Z, Moriwaki Y. Biochemistry of uridine in plasma. *Clin Chim Acta* 2011;**412**(19-20):1712–1724.

48. Nishiyama K. The role of P2Y 6 receptor in the pathogenesis of cardiovascular and inflammatory diseases. *J Pharmacol Sci* 2024;**154**(2):108–112.

49. Zhou M, Wang W, Li Y, et al. The role of P2Y6R in cardiovascular diseases and recent development of P2Y6R antagonists. *Drug Discovery Today* 2020;**25**(3):568–573.

50. Riegel AK, Faigle M, Zug S, et al. Selective induction of endothelial P2Y6 nucleotide receptor promotes vascular inflammation. *Blood* 2011;**117**(8):2548–2555.

51. Nishida M, Sato Y, Uemura A, et al. P2Y6 receptor-Galpha12/13 signalling in cardiomyocytes triggers pressure overload-induced cardiac fibrosis. *EMBO J* 2008;**27**(23):3104–3115.

52. Kauffenstein G, Tamareille S, Prunier F, et al. Central role of P2Y 6 UDP receptor in arteriolar myogenic tone. *ATVB* 2016;**36**(8):1598–1606.

53. Dale NC, Johnstone EKM, Pfleger KDG. GPCR heteromers: an overview of their classification, function and physiological relevance.*Front Endocrinol* 2022;**13**(August):1–13.

54. Guo X, Li Q, Pi S, Xia Y, Mao L. G protein-coupled purinergic P2Y receptor oligomerization: pharmacological changes and dynamic regulation. *Biochem Pharmacol* 2021;**192**(July):114689.

55. Rukavina Mikusic NL, Silva MG, Pineda AM, Gironacci MM. Angiotensin receptors heterodimerization and trafficking: how much do they influence their biological function? *Front Pharmacol* 2020;**11**(August):1–20.

56. Quitterer U, Fu X, Pohl A, Bayoumy KM, Langer A, AbdAlla S. Beta-Arrestin1 prevents preeclampsia by downregulation of mechanosensitive AT1-B2 receptor heteromers. *Cell* 2019;**176**(1-2):318–333.e19 .

57. Abdalla S, Lother H, Langer A, El Faramawy Y, Quitterer U. Factor XIIIA transglutaminase crosslinks AT1 receptor dimers of monocytes at the onset of atherosclerosis. *Cell* 2004;**119**(3):343–354.

58. Plouffe B, Thomsen ARB, Irannejad R. Emerging role of compartmentalized G protein-coupled receptor signaling in the cardiovascular field. *ACS Pharmacol Transl Sci* 2020;**3**(2):221–236.

59. Bian J, Zhang S, Yi M, Yue M, Liu H. The mechanisms behind decreased internalization of angiotensin II type 1 receptor. *Vasc Pharmacol* 2018;**103-105**(January):1–7.

60. Rozenfeld R, Gupta A, Gagnidze K, et al. AT1R-CB1 R heteromerization reveals a new mechanism for the pathogenic properties of angiotensin II. *EMBO J* 2011;**30**(12):2350–2363.

61. Breitwieser GE. G protein–Coupled receptor oligomerization. *Circ Res* 2004;**94**(1):17–27.

62. Jackson KL, Head GA, Gueguen C, Stevenson ER, Lim K, Marques FZ. Mechanisms responsible for genetic hypertension in Schlager BPH/2 mice. *Front Physiol* 2019;**10**(October):1311.

63. Iwao H, Nakamura N, Kim S, Ikemoto F, Yamamoto K, Schlager G. Renin-angiotensin system in genetically hypertensive mice. *Jpn Circ J* 1984;**48**(11):1270–1279.

64. Yang T, Xu C. Physiology and pathophysiology of the intrarenal renin-angiotensin system: an update. *JASN* 2017;**28**(4):1040–1049.

65. Noh MR, Jang HS, Kim J, Padanilam BJ. Renal sympathetic nerve-derived signaling in acute and chronic kidney diseases. *Int J Mol Sci* 2020;**21**(5):1647.

66. Uddin M, Harris-Nelson N. Renin activity and angiotensin I concentration in genetically selective inbred line of hypertensive mice. *Biochem Biophys Res Commun* 2004;**316**(3):842–844.

67. Patel SK, Velkoska E, Freeman M, Wai B, Lancefield TF, Burrell LM. From gene to protein-experimental and clinical studies of ACE2 in blood pressure control and arterial hypertension. *Front Physiol* 2014;**5**(June):1–12.

68. Kuriakose J, Montezano AC, Touyz RM. ACE2/Ang-(1-7)/Mas1 axis and the vascular system: vasoprotection to COVID-19-associated vascular disease. *Clin Sci* 2021;**135**(2):387–407.

69. Jackson KL, Marques FZ, Watson AMD, et al. A novel interaction between sympathetic overactivity and aberrant regulation of renin by miR-181a in BPH/2 J genetically hypertensive mice. *Hypertension* 2013;**62**(4):775–781.

70. Phillips MI, de Oliveira EM. Brain renin angiotensin in disease. *J Mol Med* 2008;**86**(6):715–722.